Radiology: Imaging Cancer

ORIGINAL RESEARCH

Deformable Mapping of Rectal Cancer Whole-Mount Histology with Restaging MRI at Voxel Scale: A Feasibility Study

João Miranda, MD • Jon S. Heiselman, PhD* • Canan Firat, MD • Jayasree Chakraborty, PhD • Rami S. Vanguri, PhD • Antonildes N. Assuncao, Jr, MD, PhD • Josip Nincevic, MD • Tae-Hyung Kim, MD, MS • Lee Rodriguez, MS • Nil Urganci, MD • Mithat Gonen, PhD • Julio Garcia-Aguilar, MD, PhD • Marc J. Gollub, MD • Jinru Shia, MD • Natally Horvat, MD, PhD*

From the Departments of Radiology (J.M., J.N., T.H.K., L.R., M.J.G., N.H.), Surgery (J.S.H., J.C., M.G., J.G.A.), and Pathology (C.F., N.U., J.S.), Memorial Sloan-Kettering Cancer Center, 1275 York Ave, New York, NY 10065; Department of Radiology, University of São Paulo, São Paulo, Brazil (J.M., A.N.A., N.H.); Department of Medicine, Division of Precision Medicine, NYU Grossman School of Medicine, New York, NY (R.S.V.); Department of Biomedical Engineering, Vanderbilt University, Nashville, Tenn (J.S.H.); Research and Education Institute, Hospital Sirio-Libanes, São Paulo, Brazil (A.N.A.); and Department of Radiology, Mayo Clinic, Rochester, Minn (J.M., N.H.). Received March 15, 2024; revision requested May 1; revision received July 24; accepted September 9. **Address correspondence to** N.H. (email: *horvat.natally@mayo.edu*).

*J.M. and J.S.H. equally contributed to this work.

Supported in part by the National Cancer Institute Cancer Center Core Grant (grant no. P30 CA008748) to the Society of Memorial Sloan Kettering (MSK) (principal investigator: N.H.); the Radiological Society of North America (RSNA) Research & Education (R&E) Foundation Bayer Healthcare/RSNA Research Seed Grant (grant no. RSD2302; principal investigator: N.H.). The content is solely the responsibility of the authors and does not necessarily represent the official views of the RSNA R&E Foundation. Additional support from the Colorectal Cancer Research Center at MSK and Coordination for the Improvement of Higher Education Personnel (CAPES) (principal investigator: J.M.).

Conflicts of interest are listed at the end of this article.

Radiology: Imaging Cancer 2024; 6(6):e240073 • https://doi.org/10.1148/rycan.240073 • Content codes: GI MR OI

Purpose: To develop a radiology-pathology coregistration method for 1:1 automated spatial mapping between preoperative rectal MRI and ex vivo rectal whole-mount histology (WMH).

Materials and Methods: This retrospective study included consecutive patients with rectal adenocarcinoma who underwent total neoadjuvant therapy followed by total mesorectal excision with preoperative rectal MRI and WMH from January 2019 to January 2022. A gastrointestinal pathologist and a radiologist established three corresponding levels for each patient at rectal MRI and WMH, subsequently delineating external and internal rectal wall contours and the tumor bed at each level and defining eight point-based landmarks. An advanced deformable image coregistration model based on the linearized iterative boundary reconstruction (LIBR) approach was compared with rigid point-based registration (PBR) and state-of-the-art deformable intensity-based multiscale spectral embedding registration (MSERg). Dice similarity coefficient (DSC), modified Hausdorff distance (MHD), and target registration error (TRE) across patients were calculated to assess the coregistration accuracy of each method.

Results: Eighteen patients (mean age, 54 years ± 13 [SD]; nine female) were included. LIBR demonstrated higher DSC versus PBR for external and internal rectal wall contours and tumor bed (external: 0.95 ± 0.03 vs 0.86 ± 0.04, respectively, $P < .001$; internal: 0.71 ± 0.21 vs 0.61 ± 0.21, $P < .001$; tumor bed: 0.61 ± 0.17 vs 0.52 ± 0.17, $P = .001$) and versus MSERg for internal rectal wall contours (0.71 ± 0.21 vs 0.63 ± 0.18, respectively; $P < .001$). LIBR demonstrated lower MHD versus PBR for external and internal rectal wall contours and tumor bed (external: 0.56 ± 0.25 vs 1.68 ± 0.56, respectively, $P < .001$; internal: 1.00 ± 0.35 vs 1.62 ± 0.59, $P < .001$; tumor bed: 2.45 ± 0.99 vs 2.69 ± 1.05, $P = .03$) and versus MSERg for internal rectal wall contours (1.00 ± 0.35 vs 1.62 ± 0.59, respectively; $P < .001$). LIBR demonstrated lower TRE (1.54 ± 0.39) versus PBR (2.35 ± 1.19, $P = .003$) and MSERg (2.36 ± 1.43, $P = .03$). Computation time per WMH slice for LIBR was 35.1 seconds ± 12.1.

Conclusion: This study demonstrates feasibility of accurate MRI-WMH coregistration using the advanced LIBR method.

Supplemental material is available for this article.

Colorectal cancer is the third most common cancer and the second leading cause of cancer deaths worldwide (1). While there is an overall downward trend in colorectal cancer incidence and mortality, there is an alarming increase in the rate of early-onset colorectal cancer among young adults (1–3). Survivors of early-onset colorectal cancer bear a higher annual economic burden as well as increased employment disability and productivity losses (4), stemming from the long-term toxicity of therapy in current standard-of-care treatment.

Traditionally, neoadjuvant chemoradiotherapy followed by total mesorectal excision—and systemic adjuvant chemotherapy, if needed, for high-risk patients—has been the main treatment for locally advanced rectal cancer. Recently, total neoadjuvant therapy, in which systemic chemotherapy in combination with chemoradiotherapy are performed before surgery, has gained prominence due to better rates of pathologic complete response, enhanced patient outcomes (4), and higher rates of nonsurgical cure (sustained clinical complete response) observed in up to approximately 50% of patients enrolled in nonoperative management (5). Although encouraging, predicting which individuals can safely avoid surgery is challenging using current methods. Therefore, nonoperative management is performed in only a few specialized cancer centers. Digital rectal examination, endoscopy, and MRI are essential components of restaging assessment after neoadjuvant therapy; however, there is subjective interpretation and lack of uniform performance standards, leading to inconsistent interreader reliability (6–9). This variability further limits the widespread use of nonoperative management.

Currently, radiologists rely predominantly on T2-weighted imaging and, in some institutions, diffusion-weighted imaging for restaging MRI (10,11). However, there is varying diagnostic performance and interreader agreement with these imaging

Abbreviations

DSC = Dice similarity coefficient, LIBR = linearized iterative boundary reconstruction, MHD = modified Hausdorff distance, MSERg = multiscale spectral embedding registration, PBR = point-based registration, TRE = target registration error, WMH = whole-mount histology

Summary

Accurate coregistration of preoperative MRI and whole-mount histology was feasible using an advanced deformable image registration technique in patients with rectal adenocarcinoma.

Key Points

- Advanced regularized Kelvinlet linearized iterative boundary reconstruction (LIBR) demonstrated higher accuracy over traditional rigid point-based registration and state-of-the-art multiscale spectral embedding registration (MSERg) (eg, target registration error, 1.54 mm ± 0.39 [SD] vs 2.35 mm ± 1.19 and 2.36 mm ± 1.43, respectively; $P < .05$) in aligning MRI with whole-mount histology in patients with rectal adenocarcinoma.
- LIBR coregistration also achieved a 40-fold improvement in computation time per whole-mount histology slice over MSERg (35.1 seconds ± 12.1 vs 1452.3 seconds ± 24.6, respectively; $P < .001$).
- LIBR coregistration is promising to guide MRI-to-pathology reference standard mapping for supervised machine learning toward improving MRI assessment of treatment response in rectal cancer.

Keywords

MR Imaging, Abdomen/GI, Rectum, Oncology

sequences (6–9,12). While several studies have investigated the added value of supplementary tools, including radiomics (13,14), artificial intelligence (15,16), and dynamic contrast-enhanced MRI (17), to increase MRI diagnostic performance in predicting treatment response (18), only a few included a reliable reference standard such as whole-mount histology (WMH).

WMH has the potential to provide a comprehensive evaluation of the entire rectum, preserving crucial spatial distribution of the structures. It serves as a fundamental reference point for validating and calibrating rectal MRI techniques and imaging assessment. Early in the application of rectal MRI, Brown et al (19,20) used WMH as the reference standard to define key landmarks, as well as imaging criteria, for preoperative baseline high-resolution MRI assessment. Since then, however, only a few studies have used WMH to assess restaging rectal MRI performance (21–23). Additionally, there is a lack of robust fusion strategies using WMH and rectal MRI, with only two reported pilot studies (24,25). Both used rigid transformations that cannot account for rectal tissue deformations between in vivo imaging and postoperative histologic processing.

To provide a foundation for accurate treatment response evaluation after neoadjuvant therapy, the current study aimed to develop a radiology-pathology coregistration method for 1:1 automated spatial mapping between preoperative rectal MRI and ex vivo rectal WMH.

Materials and Methods

Study Sample

This retrospective single-institution study was approved by the institutional review board with a waiver for written informed consent and complied with the United States Health Insurance Portability and Accountability Act.

The institutional database was searched for consecutive patients with rectal adenocarcinoma who underwent neoadjuvant therapy followed by total mesorectal excision at our institution from January 2019 to January 2022 and who had available WMH specimens. Of the initial 150 patients identified, 132 were excluded (99 because their pathology slices did not fit into a single whole-mount cassette, 30 because presurgical MRI data were unavailable, and three because of severe artifacts) (Fig 1). Some included patients (seven) were previously reported in a study evaluating the performance of diffusion-weighted MRI in detecting viable extramural venous invasion and tumor deposit in patients with locally advanced rectal cancer after neoadjuvant therapy, using WMH specimens as a reference (21).

In Vivo Rectal MRI Protocol

Restaging rectal MRI examinations were performed using a 1.5- or 3.0-T scanner (Discovery MR750, Optima MR450w, Signa EXCITE, or Signa HDxt; GE HealthCare) equipped with a phased-array coil. Images were acquired using three orthogonal planes of the pelvis for anatomic orientation. Initially, T2-weighted sagittal images of the rectum were obtained to localize the tumor and enable the planning of axial section acquisitions. Subsequently, T2-weighted axial images of the pelvis were acquired in a plane perpendicular to the rectal wall (T2-weighted axial oblique plane), including the tumor and 5 cm above and below the tumor (26). The T2-weighted axial oblique plane had a field of view of 180 × 180 mm, a scan matrix of 512 × 512, an in-plane resolution of 0.35 × 0.35 mm, echo times from 79 to 125 msec, and repetition times from 2500 to 6562 msec. The section thickness was consistently 3 mm with section spacing of 4 mm, and the flip angle was fixed at 111° to ensure clear T2-weighted imaging. If the tumor was near or involved the anal canal, coronal imaging of the anal canal was also performed, using similar imaging parameters as those for T2-weighted axial imaging.

Postcontrast sequences were not used due to their limited acceptance and use in both baseline and restaging settings (18,27,28). Conversely, diffusion-weighted imaging has proven beneficial for identifying viable tumor within the tumor bed (29). In our study, we opted to segment the tumor bed using T2-weighted imaging, considering its superior spatial resolution for this specific purpose.

Whole-Mount Histology

The rationale of WMH is to display the tumor and its relationship to other histologic structures on the same horizontal plane. We retrospectively assessed the WMH slides, and the following methodologic workflow was executed. First, the rectal cancer resection specimen was kept intact and unopened in formalin for more than 48 hours. Then, circumferential margins were marked with different ink colors to enable proper orientation (Fig 2). Subsequently, starting from the distal point to the proximal end, the entire tumor region was sliced transversely to obtain 4-mm-thick WMH slices (21). Each WMH slice was photographed and placed into a megacassette (approximately five times larger than a regular tissue cassette). Slides were then stained with hematoxylin-eosin. Each stained

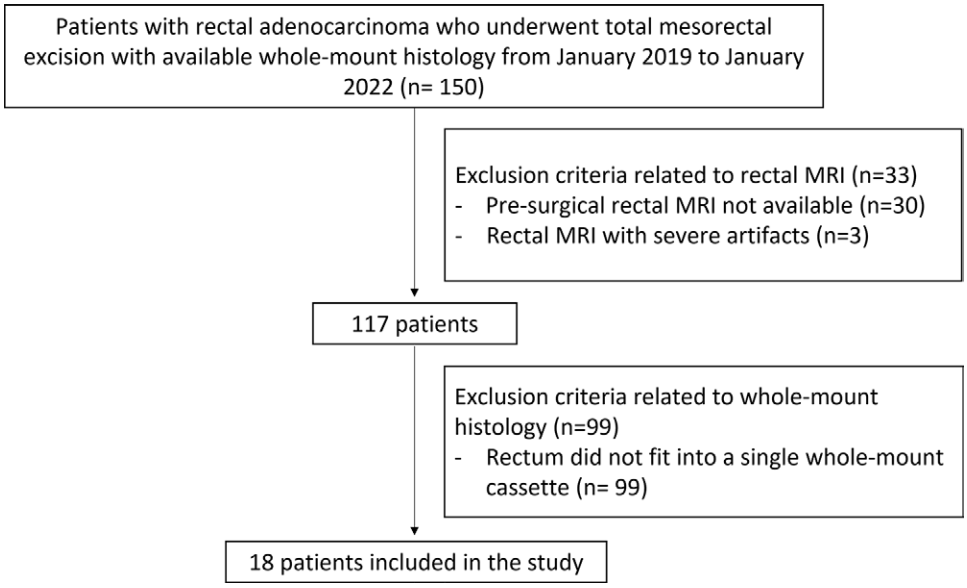

Figure 1: Flowchart of patient inclusion. This retrospective study included consecutive patients with rectal adenocarcinoma who underwent total mesorectal excision at our institution from January 2019 to January 2022 and who had available whole-mount histology (WMH) specimens. The exclusion criteria were as follows: WMH slices not fitting into a single whole-mount cassette, presurgical MRI data unavailable, and severe restaging MRI artifacts.

slide was digitized to facilitate side-by-side comparison with rectal MR images.

Image Segmentation and Landmarks

Digitized WMH slides served as the reference standard for the restaging rectal MR images (T2-weighted images) using the high-resolution oblique sequence, perpendicular to the tumor bed. A gastrointestinal pathologist (C.F., with 7 years of experience) and a radiologist (J.M., with 6 years of experience) performed side-by-side review of WMH and MRI to achieve precise point-by-point correlation between WMH and MRI, establishing three corresponding levels for each patient at WMH and MRI—midpoint of the tumor bed, one section above, and one section below—and then manually delineating the external rectal contour (the external edge of the muscularis propria), internal rectal contour (inner aspect of the mucosa), and tumor bed at each designated level. To delineate the tumor bed accurately, the radiologist analyzed the baseline MRI scan using the T2-weighted imaging sequence, which is known to enhance the delineation of the tumor bed at restaging MRI (30). Furthermore, the radiologist and pathologist annotated eight corresponding point-based landmarks in each modality along the internal and external borders of the rectal wall in the anterior, posterior, leftward, and rightward directions (Fig 3). In addition to the eight landmarks, three additional corresponding target points were identified to validate accuracy by selecting three corresponding validation points anatomically localized between the external and internal rectal contours. Target points were identified along well-discriminated common vein positions, texture patterns, and anatomic geometric relationships visible in both radiologic and pathologic images. These target points were selected within the rectal wall in the muscularis propria layer. The specific features selected as target points differed among patients depending on the best discriminatory point between radiology and pathology.

An experienced gastrointestinal pathologist (J.S., with 23 years of experience) was consulted for equivocal pathology slides, and final determinations were based on consensus. Similarly, for equivocal MR images, an experienced gastrointestinal radiologist (N.H., with 10 years of experience) was consulted.

Radiology-Pathology Image Coregistration

Due to intermodality differences between radiology and pathology, we assumed that contour-based coregistration methods using continuum models of soft tissue deformation to constrain realistic tissue behavior would be more reliable than intensity-based coregistration methods. Thus, we developed an advanced multimodal radiology-pathology contour-based coregistration workflow to enable spatial mapping between WMH and MRI. An advanced deformable image registration method was developed using regularized Kelvlinet solutions to linear elastic biomechanics (31) to establish a deformation basis that is optimized within a linearized iterative boundary reconstruction (LIBR) framework (32) to optimize agreement between rectal wall contours. This proposed approach maintains biomechanical consistency when estimating deformation between WMH tissue samples and MR images with excellent computational efficiency. Details are included in the Biomechanical Model, Deformation Energy, and Deformable Registration Model sections in Appendix S1. Regularized Kelvinlets establish a highly efficient, closed-form decomposition of the underlying mathematical equations that govern soft tissue mechanics. Incorporating regularized Kelvinlets into the LIBR approach subsequently leverages this deformation basis to rapidly and accurately reconstruct tissue deformations at low computational expense.

Figure 3 outlines the workflow of the proposed coregistration method. The workflow begins with rigid point-based registration (PBR) with rescaling using a standard singular value decomposition method (33) to register the eight point-based landmarks that were manually annotated on the external and internal rectal

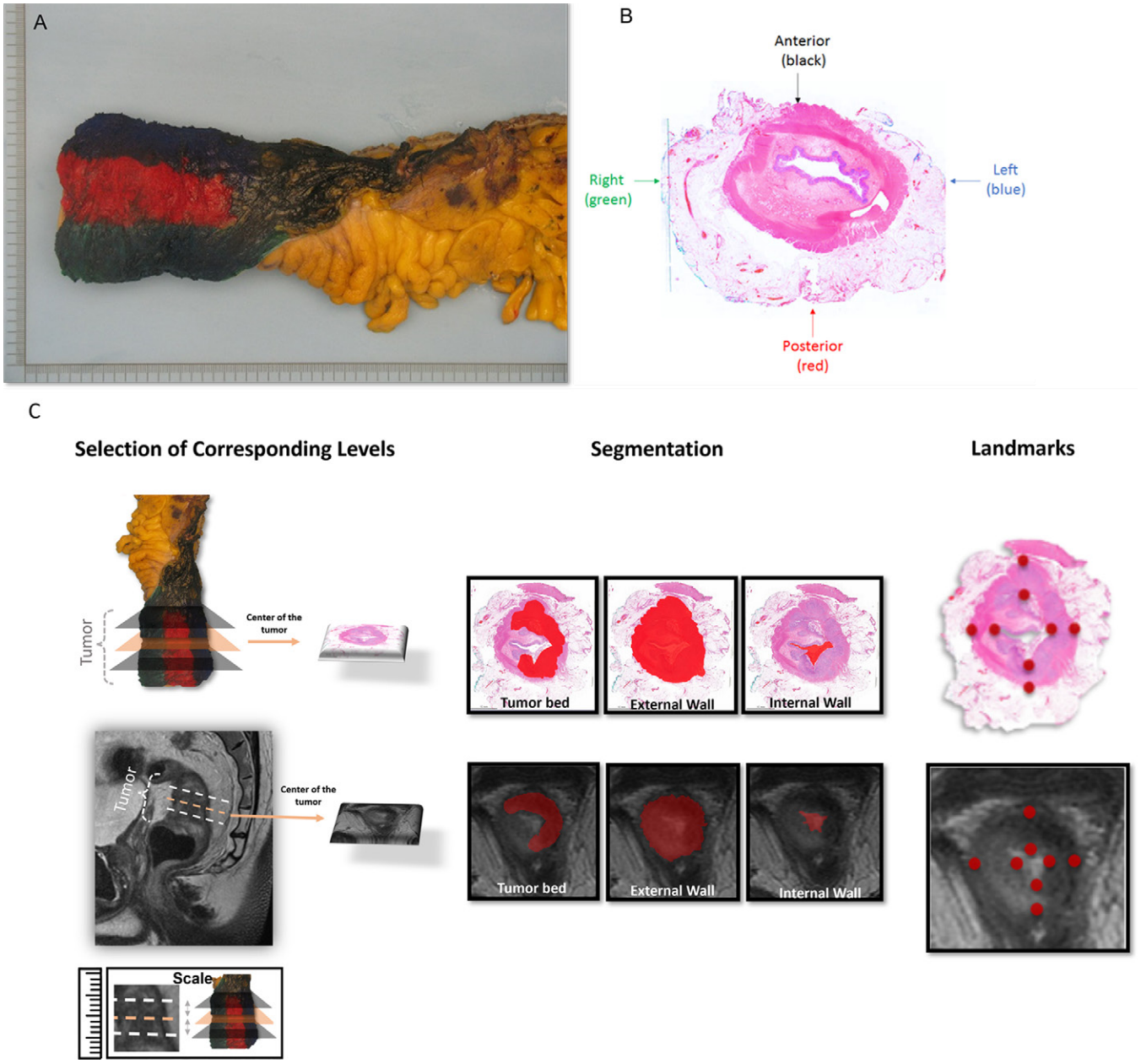

Figure 2: Demarcation of a standard total mesorectal excision specimen on **(A, B)** surgical and whole-mount histology (WMH) slices and **(C)** radiology-pathology workflow of segmentation and landmark definition. **(A)** Circumferential margins of the rectal cancer resection specimen were marked with different ink colors to distinguish anterior and posterior and right and left regions of the specimen and enable proper orientation. **(B)** WMH slice of the total mesorectal excision specimen demonstrates the color code that was used to guide the spatial localization of the rectum portions, as follows: black = anterior, red = posterior, blue = left, and green = right. **(C)** A gastrointestinal pathologist and a radiologist conducted a collaborative review of WMH and MR images to ensure precise correspondence between pathology and high-resolution T2-weighted imaging. Three corresponding levels were established for each patient at WMH and MRI: the midpoint of the tumor bed, one slice or section above, and one slice or section below. Subsequently, both experts manually delineated the external rectal contour (the outer edge of the muscularis propria), internal rectal contour (inner aspect of the mucosa), and tumor bed at each designated level (illustrated at the midpoint level). Additionally, the radiologist and pathologist annotated eight corresponding point-based landmarks in each modality along the internal and external borders of the rectal wall, encompassing the anterior, posterior, leftward, and rightward directions.

contours in WMH and MR images and thus initialize the multimodal alignment. Then, the proposed regularized Kelvinlet LIBR method was used to refine differences in radiology-pathology agreement caused by soft tissue deformations occurring between the imaging time point and the fixation of the resected specimen in formalin.

Separately from our proposed contour-based LIBR coregistration workflow, a second intensity-based deformable image registration method, the state-of-the-art multiscale spectral embedding registration (MSERg) (34) method, was evaluated. This method uses a radiomic-based intensity pattern matching approach to detect common independent components of imaging signal between modalities and drive a B-spline deformation model.

Statistical Analysis

Coregistration accuracy for each coregistration method (PBR, LIBR, and MSERg) was evaluated using three measures. The Dice similarity coefficient (DSC) was used to assess overlap in the segmented tumor bed and external and internal rectal contours between radiologic and pathologic modalities. The modified Hausdorff distance (MHD) was used to assess the

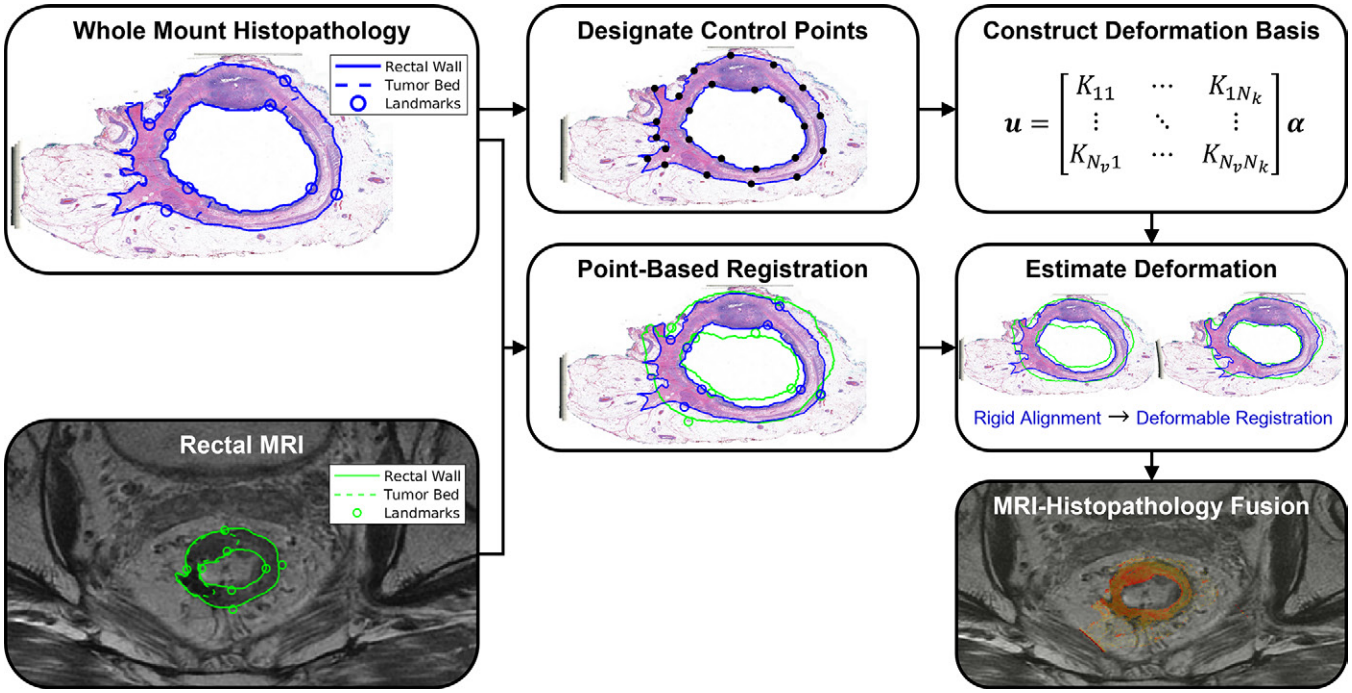

Figure 3: Coregistration workflow for the proposed linearized iterative boundary reconstruction (LIBR) MRI-histopathology fusion method after segmentation and landmark characterization as demonstrated in Figure 2. Prior to coregistration, eight point-based landmarks are annotated on the external and internal rectal contours on each MR and whole-mount histopathology (WMH) image. A series of regularized Kelvinlet control points is then distributed across the external and internal rectal contours, from which a biomechanical deformation basis is constructed. After point-based registration of landmarks, deformation of the histopathology sample relative to MRI is computed from the rectal wall contours via the LIBR approach. A series of control points are distributed across the external and internal rectal contours to establish a regularized Kelvinlet deformation basis for the WMH image. The LIBR approach estimates the deformation between WMH and MRI by maximizing the agreement between rectal wall contours subject to this deformation basis. Finally, the registered WMH is fused with MRI to indicate spatial correspondence between reference standard histopathologic features and MRI.

spatial distance to agreement of the segmented rectal contours and tumor bed between radiologic and pathologic modalities. Finally, target registration error (TRE) was assessed as the reference standard measure for spatial registration error according to the distance after coregistration between corresponding target points identified in the radiologic and pathologic images. Further details of these validation measures are provided in the Evaluation Metrics section of Appendix S1.

Mean ± SD values of DSC, MHD, and TRE were computed for each patient across each of the three axial levels, as well as averaged across the entire study sample. Statistical differences in average accuracy between our LIBR method and the PBR or MSERg methods were tested for significance via paired *t* tests, at a significance level of $\alpha = .05$.

Computation time per pathology slide for each coregistration method was also measured.

Coregistration methods and statistical analyses were performed in MATLAB 2022b (MathWorks).

Results

Patient Characteristics

The final study sample (Table 1) comprised 18 patients (mean age, 54 years ± 13 [SD]; nine male patients [50%] and nine female patients [50%]). The majority underwent total neoadjuvant therapy (15 of 18, 83%) (six with induction chemotherapy and nine with consolidation chemotherapy), while the remaining (three of 18, 17%) underwent only chemotherapy. Chemotherapy regimens used in total neoadjuvant therapy included fluorouracil, leucovorin, and oxaliplatin (ie, mFOLFOX), capecitabine and oxaliplatin (ie, CAPOX), or fluorouracil, leucovorin, and oxaliplatin (ie, FLOX). Standard chemoradiation involved long-course radiation therapy (45 Gy in 1.8-Gy fractions to the pelvis, with a 5.4-Gy boost to the tumor) with concurrent fluorouracil or capecitabine.

The mean duration between MRI and resection was 22.8 days ± 10.1, with a range from 4 to 38 days. Most patients (12 of 18, 67%) underwent low anterior resection. When assessing the pathologic tumor stage (pT), the majority (10 of 18, 56%) were classified as pT3. A substantial portion of the patient sample (14 of 18, 78%) showed no nodal involvement, no metastasis (17 of 18, 94%), no tumor deposits (14 of 18, 78%), and no extramural vascular invasion (17 of 18, 94%).

Coregistration Results

Contour overlap.— LIBR had a higher DSC compared with PBR for the external rectal contour, internal rectal contour, and tumor bed (external rectal contour: 0.95 ± 0.03 vs 0.86 ± 0.04, respectively, $P < .001$; internal rectal contour: 0.71 ± 0.21 vs 0.61 ± 0.21, $P < .001$; tumor bed: 0.61 ± 0.17 vs 0.52 ± 0.17, $P = .001$).

Comparing LIBR and MSERg, LIBR demonstrated a higher DSC for the internal rectal contour (0.71 ± 0.21 vs 0.63 ± 0.18, $P < .001$), and MSERg had a higher DSC for the external contour (0.97 ± 0.02 vs 0.95 ± 0.03, $P = .04$). No evidence of a difference was observed between LIBR and MSERg in the DSC for the tumor bed ($P = .10$).

Table 1: Patient Characteristics

Characteristic	Value
Age (y)	54.1 ± 12.77
Biologic sex	
Male	9 (50)
Female	9 (50)
Neoadjuvant treatment	
Chemotherapy	3 (17)
TNT	15 (83)
Interval between neoadjuvant therapy and restaging MRI (d)	58 ± 35
Interval between restaging MRI and surgery (d)	32 ± 25
Surgery type	
APR	6 (33)
LAR	12 (67)
Tumor location at MRI	
Upper	7 (39)
Middle	7 (39)
Lower	4 (22)
yp Tumor characteristic	
Nonmucinous	18 (100)
Other	0 (0)
ypT	
0	1 (5.6)
1	2 (11)
2	5 (28)
3	10 (56)
ypN	
N0	14 (78)
N+	4 (22)
pM	
M0	17 (94)
M+	1 (5.6)
yp Tumor deposit	4 (22)
yp Extramural vascular invasion	1 (5.6)

Note.—Continuous data are presented as means ± SDs, and categorical variables are presented as numbers of patients, with percentages in parentheses. A total of 18 patients were in the study cohort. APR = abdominoperineal resection, LAR = low anterior resection, pM = pathologic metastasis stage, pN = pathologic node stage, pT = pathologic tumor stage, TNT = total neoadjuvant therapy, yp = pathologic classification at posttreatment assessment.

Distance to agreement.— LIBR demonstrated a lower MHD compared with PBR for the external rectal contour, internal rectal contour, and tumor bed (external rectal contour: 0.56 ± 0.25 vs 1.68 ± 0.56, respectively, $P < .001$; internal rectal contour: 1.00 ± 0.35 vs 1.62 ± 0.59, $P < .001$; tumor bed: 2.45 ± 0.99 vs 2.69 ± 1.05, $P = .03$).

Additionally, LIBR had a lower MHD compared with MSERg for the internal rectal contour (1.00 ± 0.35 vs 1.62 ± 0.59, respectively; $P < .001$), with no evidence of a difference in MHD for the external rectal contour or tumor bed between LIBR and MSERg.

Target registration error.— Regarding TRE, LIBR demonstrated lower values (1.54 ± 0.39) compared with both PBR (2.35 ± 1.19, $P = .003$) and MSERg (2.36 ± 1.43, $P = .03$).

Table 2 provides quantitative details of the accuracy of each coregistration method.

Figure 4 provides a visualization of the alignment quality achieved by each coregistration method, allowing for a straightforward visual comparison of each method's effectiveness in different scenarios (best-, average-, and worst-performing cases within our study sample in terms of alignment). Figure 5 illustrates the distribution of accuracy values for each coregistration method across the study sample. Tables S1–S3 provide DSC, MHD, and TRE values, respectively, at the patient level.

Computation Time

Computation time per WMH slice was lower for PBR compared with LIBR (0.0003 seconds ± 0.0004 vs 35.1 seconds ± 12.1, respectively; $P < .001$) and for LIBR compared with MSERg (35.1 seconds ± 12.1 vs 1452.3 seconds ± 24.6, respectively; $P < .001$). Each coregistration method differed by more than one order of magnitude in computation speed. Table S4 provides computation times at the patient level.

Discussion

There is an urgent need to establish a precise reference standard to enable accurate imaging evaluation of treatment response after neoadjuvant therapy in patients with rectal cancer. WMH provides a comprehensive evaluation of the entire rectum, preserving crucial spatial distribution of the structures. Thus, we developed a radiology-pathology coregistration method for accurate 1:1 automated spatial mapping between preoperative restaging rectal MRI after neoadjuvant therapy and ex vivo rectal WMH. Our advanced biomechanically constrained contour-based LIBR deformable coregistration method outperformed rigid PBR, as well as state-of-the-art MSERg, an intensity-based deformable coregistration method. LIBR demonstrated higher DSC versus PBR for external and internal rectal contours and tumor bed (external: 0.95 ± 0.03 vs 0.86 ± 0.04, respectively, $P < .001$; internal: 0.71 ± 0.21 vs 0.61 ± 0.21, $P < .001$; tumor bed: 0.61 ± 0.17 vs 0.52 ± 0.17, $P = .001$) and versus MSERg for internal rectal contours (0.71 ± 0.21 vs 0.63 ± 0.18, $P < .001$). LIBR demonstrated lower MHD versus PBR for external and internal rectal contours and tumor bed (external: 0.56 ± 0.25 vs 1.68 ± 0.56, respectively, $P < .001$; internal: 1.00 ± 0.35 vs 1.62 ± 0.59, $P < .001$; tumor bed: 2.45 ± 0.99 vs 2.69 ± 1.05, $P = .03$) and versus MSERg for internal rectal contours (1.00 ± 0.35 vs 1.62 ± 0.59, respectively; $P < .001$). LIBR demonstrated lower TRE (1.54 ± 0.39) versus PBR (2.35 ± 1.19, $P = .003$) and MSERg (2.36 ± 1.43, $P = .03$). LIBR coregistration also achieved a 40-fold improvement in computation time per WHM slice over MSERg (35.1 seconds ± 12.1 vs 1452.3 seconds ± 24.6, respectively; $P < .001$).

In the realm of coregistering radiology images with pathology specimens, the field remains relatively specialized, with limited publications to date. The existing literature predominantly revolves around prostate cancer (35–38), with only two references to rectal cancer (24,25) and another to lung nodules (39). These

Table 2: Comparison of Different MRI–Whole-Mount Histology Coregistration Methods Using Three Measures

Parameter	PBR*	LIBR*	*P* Value (PBR vs LIBR)	MSERg*	*P* Value (LIBR vs MSERg)
DSC					
External rectal contour	0.86 ± 0.04	0.95 ± 0.03	<.001	0.97 ± 0.02	.04
Internal rectal contour	0.62 ± 0.21	0.71 ± 0.21	<.001	0.63 ± 0.18	<.001
Tumor bed	0.52 ± 0.17	0.61 ± 0.17	.001	0.58 ± 0.17	.10
MHD (mm)					
External rectal contour	1.68 ± 0.56	0.56 ± 0.25	<.001	0.86 ± 2.15	.56
Internal rectal contour	1.62 ± 0.59	1.00 ± 0.35	<.001	1.64 ± 0.50	<.001
Tumor bed	2.69 ± 1.05	2.45 ± 0.99	.03	2.66 ± 1.08	.13
TRE (mm)	2.35 ± 1.19	1.54 ± 0.39	.003	2.36 ± 1.43	.03
Computation time (sec) †	0.0003 ± 0.0004	35.1 ± 12.1	<.001	1452.3 ± 24.6	<.001

Note.—The Dice similarity coefficient (DSC) was used to assess overlap in the segmented tumor bed and external and internal rectal contours between radiologic and pathologic modalities. The modified Hausdorff distance (MHD) was used to assess the spatial distance to agreement of the segmented rectal contours and tumor bed between radiologic and pathologic modalities. Target registration error (TRE) was assessed as the reference standard measure for spatial registration error according to the distance after coregistration between corresponding target points identified in the radiologic and pathologic images. LIBR = linearized iterative boundary reconstruction, MSERg = multiscale spectral embedding registration, PBR = point-based registration.
* Values represent the means ± SDs across the entire study sample (n = 18).
† Registration time is measured per pathology slide.

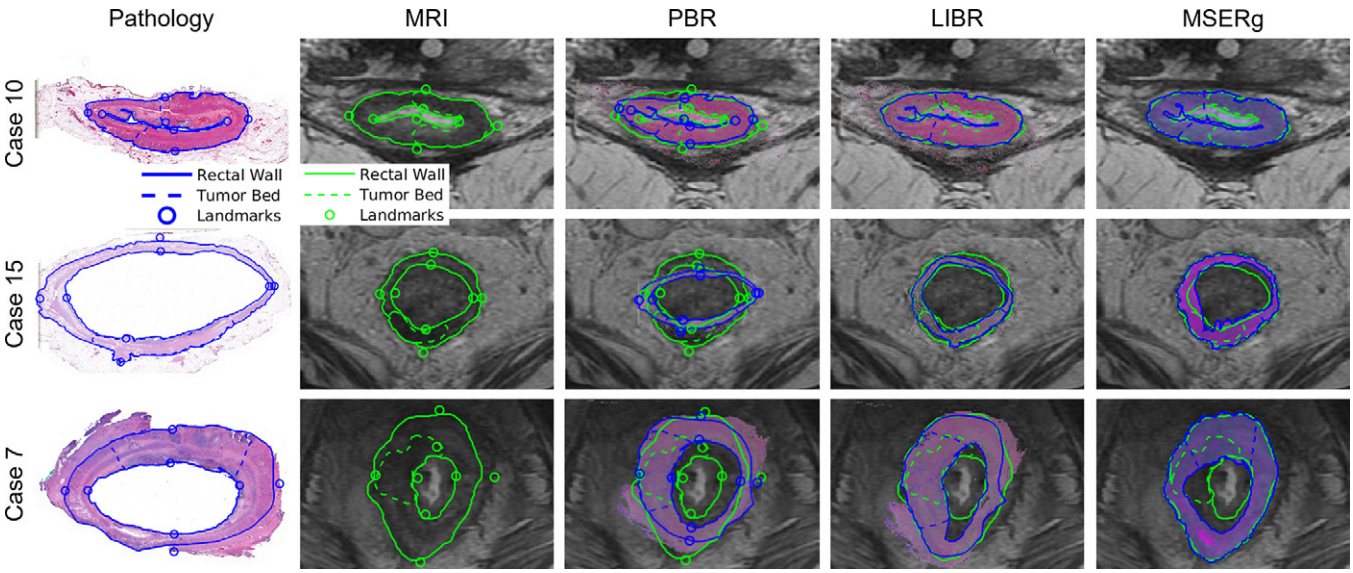

Figure 4: Visualization of the alignment quality achieved by each coregistration method. Restaging MR–whole-mount histology image fusion is shown in three representative cases. Case 10 (a 43-year-old female patient), case 15 (a 65-year-old male patient), and case 7 (a 47-year-old male patient) represent cases with the best Dice similarity coefficient, average Dice similarity coefficient, and worst Dice similarity coefficient, respectively. Between the investigated linearized iterative boundary reconstruction (LIBR), rigid point-based registration (PBR), and multiscale spectral embedding registration (MSERg) methods, LIBR produced better alignment. Note that in case 7, MSERg produced a misalignment of approximately 90° between the pathology slice and the MR image.

studies explored a range of coregistration methods, including the use of injected fiducials, thin-plate spline, and a combination of rigid and nonrigid techniques.

Only two studies proposing a coregistration technique between MRI and WMH exist in the scientific literature to date (24,25). Both studies used a rigid PBR approach that depends on manually annotated landmark positions estimated along the inner and outer walls of the rectum in both MRI and WMH. We reproduced this PBR approach as a baseline comparator for the deformable registration method we propose in this work. Whereas several deformable coregistration methods have been proposed primarily in the context of prostate cancer, comprehensively reviewed by Pham et al (25), no existing methods have been applied to coregistration of rectal WMH.

Antunes et al (24) used a rigid landmark-based registration method equivalent to our PBR comparator. Their method yielded coregistration accuracy of 1.50 mm ± 0.63 between pathology and MRI in six patients with rectal cancer; however, this level of accuracy was not reproducible in our larger sample of 18 patients, likely due to larger tissue deformations, differences in treatment response, and differences in tissue processing, despite a similar time interval from MRI to surgery. Our

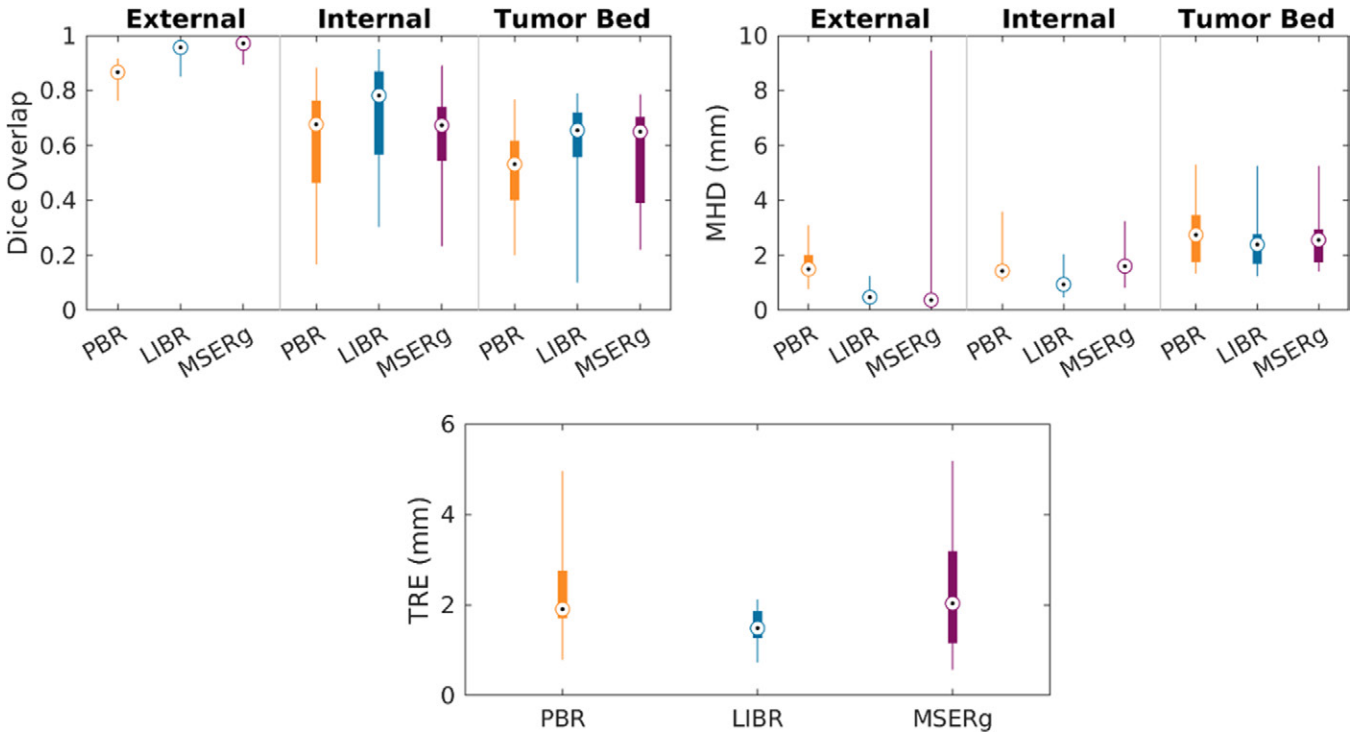

Figure 5: Distribution of accuracy values for each coregistration method across the study sample. Coregistration accuracy was assessed for our linearized iterative boundary reconstruction (LIBR) method, the rigid point-based registration (PBR) method, and the multiscale spectral embedding registration (MSERg) method using the Dice similarity coefficient (DSC), the modified Hausdorff distance (MHD), and the target registration error (TRE). The LIBR method produced lower TRE, DSC, and MHD than the rigid PBR method across all features evaluated (external rectal contour, internal rectal contour, and tumor bed) and also produced lower TRE, DSC, and MHD than MSERg along the internal rectal wall.

findings indicate that PBR, despite its initial promise, exhibited limitations in coregistration accuracy according to all accuracy metrics (ie, DSC, MHD, and TRE). While Antunes et al suggested that the radiology-pathology fusion approach could aid interpretation of restaging MRI, they found that their method was limited in distinguishing T2-weighted imaging intensity ranges between fibrotic tissue and residual cancer. Machine learning models will likely be necessary to address clinical scenarios where distinguishing between viable and nonviable tissue is critical, and accurate mapping of reference standard information from pathology at the voxel scale will be essential toward training these models.

In comparison, both deformable image registration methods (LIBR and MSERg) displayed greater accuracy in terms of DSC and MHD metrics than did PBR, with LIBR emerging as the most effective method for coregistration, especially for tumor bed and internal border segmentations. Only LIBR restored a similar level of coregistration accuracy as that reported in Antunes et al (24). MSERg, which was originally developed for registration of prostate MRI with WMH, was less accurate than LIBR. This likely arises from the dependence of MSERg on correlating cross-modality texture information, whereas LIBR depends only on geometric alignment of the rectal walls while maintaining biomechanical consistency throughout the sample; this is done by modeling soft tissue deformations in a computationally efficient manner that also minimizes dependence on patient-specific tissue properties. Although MSERg had the best DSC for the external rectal wall, overfitting is likely, and LIBR generally showed higher accuracy across all other metrics while reducing computation time more than 40-fold compared with MSERg. The overfitting behavior of MSERg arises due to this method applying a binary mask of the external rectal wall to the intensity values of both the MR and WMH images. This subsequently forces high conformity of the external contours, which may negatively impact alignments of other internal structures.

The multimodal workflow proposed for MRI and WMH coregistration builds toward new capabilities to robustly map the tumor bed habitat from high-resolution histopathology images to MRI, allowing for the creation of highly accurate reference standard labels for training machine learning models to predict residual disease at the voxel scale. Future work will use the methods developed herein to correlate reference standard labels from pathology to MRI to train artificial intelligence and radiomics models to distinguish viable from nonviable rectal tumor tissue. These models aim to improve prediction of which patients may safely avoid surgery after neoadjuvant therapy or to more precisely localize and target disease for local-regional therapy within the treatment course of rectal cancer. However, we acknowledge challenges related to pathology angulation of the surgical specimen, which can potentially differ from MRI angulation, such as large rectal specimens that may not fit into a single whole-mount megacasette and the manual effort needed to establish voxel-scale correlations. Addressing these challenges will involve exploring automated methods for aligning pathology and MR images, optimizing hardware and software to accommodate large rectal specimens, and implementing efficient algorithms to establish voxel-scale correlations, thus paving the way for more streamlined and accurate clinical applications.

The primary limitations of our study included the relatively small retrospective sample size of 18 patients, which restricts

the robustness and generalizability of our findings. Considering the feasibility phase of this study, we opted to include only patients whose entire rectum could be accommodated within one megacassette. This decision, while reducing the sample size, facilitated a more homogeneous method. Additionally, the retrospective nature of the study with a mean interval between MRI and surgery of 22 days presented challenges in the coregistration process. To address concerns about potential orientation discrepancies between tissue slices and MRI sections, our method focused on identifying and annotating specific anatomic landmarks and target points visible in both modalities. This approach allowed for accurate validation and alignment between WMH and MR images, accounting for any potential differences in orientation. While subjective interpretation may play a role to some extent, the extensive experience of the reviewers helped ensure consistency and reliability in the correlation process. This concern is further compounded by inherent methodologic challenges, such as the limited capacity for PBR to account for soft tissue deformation and the need for further refinement to improve automatability of coregistration methods. Technical and operational constraints, including imaging resolution, precision of segmentation techniques, and potential for human error in landmark annotation, likely had a substantial impact on the results. Furthermore, as this was a single-center study, our results may predominantly reflect local practices and patient demographics, potentially limiting generalizability.

In conclusion, we proposed a mechanics-based deformable registration algorithm for multimodal coregistration between MRI and WMH in rectal cancer and found that the proposed technique outperforms state-of-the-art techniques for rigid and deformable pathology image fusion. While a multicenter study with a larger patient sample and prospectively assessing MRI-WMH using controlled slice angulation directed by MRI are crucial for optimizing the workflow, improving alignment between the modalities and enhancing generalizability, this study demonstrates the feasibility of this approach, laying a solid foundation for future endeavors.

Acknowledgments: The authors thank Joanne Chin, MFA, ELS, for editing the manuscript.

Author contributions: Guarantors of integrity of entire study, **J.M., J.S.H., J.N., N.H.**; study concepts/study design or data acquisition or data analysis/interpretation, all authors; manuscript drafting or manuscript revision for important intellectual content, all authors; approval of final version of submitted manuscript, all authors; agrees to ensure any questions related to the work are appropriately resolved, all authors; literature research, **J.M., J.S.H., J.C., R.S.V., J.N., T.H.K., L.R., N.U., M.J.G., J.S., N.H.**; clinical studies, **J.M., J.S.H., J.C., J.N., J.G.A., M.J.G., J.S., N.H.**; statistical analysis, **J.S.H., J.C., R.S.V., J.N., L.R., M.G.**; and manuscript editing, **J.M., J.S.H., C.F., J.C., R.S.V., A.N.A., J.N., T.H.K., L.R., M.G., J.G.A., M.J.G., N.H.**

Disclosures of conflicts of interest: **J.M.** No relevant relationships. **J.S.H.** No relevant relationships. **C.F.** No relevant relationships. **J.C.** No relevant relationships. **R.S.V.** No relevant relationships. **A.N.A.** No relevant relationships. **J.N.** Financial support from Memorial Sloan Kettering Cancer Center to present at and attend the 2024 European Congress of Radiology. **T.H.K.** No relevant relationships. **L.R.** No relevant relationships. **N.U.** No relevant relationships. **M.G.** Support from the National Institutes of Health (grant no. P30 CA008748), paid to author's employer. **J.G.A.** Stock in Intuitive Surgical. **M.J.G.** No relevant relationships. **J.S.** No relevant relationships. **N.H.** One-time consultant agreement with Guerbet (February 2023); one-time speaker agreement with Bayer (September 2022) and Guerbet (May 2024); travel support from Guerbet (February 2023 for Society of Abdominal Radiology and May 2024 for Jornada Paulista de Radiologia).

References

1. Sung H, Ferlay J, Siegel RL, et al. Global Cancer Statistics 2020: GLOBOCAN Estimates of Incidence and Mortality Worldwide for 36 Cancers in 185 Countries. CA Cancer J Clin 2021;71(3):209–249.
2. Siegel RL, Torre LA, Soerjomataram I, et al. Global patterns and trends in colorectal cancer incidence in young adults. Gut 2019;68(12):2179–2185.
3. Vuik FE, Nieuwenburg SA, Bardou M, et al. Increasing incidence of colorectal cancer in young adults in Europe over the last 25 years. Gut 2019;68(10):1820–1826.
4. Kong JC, Soucisse M, Michael M, et al. Total neoadjuvant therapy in locally advanced rectal cancer: a systematic review and metaanalysis of oncological and operative outcomes. Ann Surg Oncol 2021;28(12):7476–7486.
5. Garcia-Aguilar J, Patil S, Gollub MJ, et al. Organ preservation in patients with rectal adenocarcinoma treated with total neoadjuvant therapy. J Clin Oncol 2022;40(23):2546–2556.
6. Nahas SC, Rizkallah Nahas CS, Sparapan Marques CF, et al. Pathologic complete response in rectal cancer: can we detect it? lessons learned from a proposed randomized trial of watch-and-wait treatment of rectal cancer. Dis Colon Rectum 2016;59(4):255–263.
7. Siddiqui MR, Gormly KL, Bhoday J, et al. Interobserver agreement of radiologists assessing the response of rectal cancers to preoperative chemoradiation using the MRI tumour regression grading (mrTRG). Clin Radiol 2016;71(9):854–862.
8. Sclafani F, Brown G, Cunningham D, et al. Comparison between MRI and pathology in the assessment of tumour regression grade in rectal cancer. Br J Cancer 2017;117(10):1478–1485.
9. Patel UB, Brown G, Rutten H, et al. Comparison of magnetic resonance imaging and histopathological response to chemoradiotherapy in locally advanced rectal cancer. Ann Surg Oncol 2012;19(9):2842–2852.
10. Lee S, Kassam Z, Baheti AD, et al. Rectal cancer lexicon 2023 revised and updated consensus statement from the Society of Abdominal Radiology Colorectal and Anal Cancer Disease-Focused Panel. Abdom Radiol (NY) 2023;48(9):2792–2806.
11. Chandramohan A, Siddiqi UM, Mittal R, et al. Diffusion weighted imaging improves diagnostic ability of MRI for determining complete response to neoadjuvant therapy in locally advanced rectal cancer. Eur J Radiol Open 2020;7:100223.
12. Yuval JB, Patil S, Gangai N, et al. MRI assessment of rectal cancer response to neoadjuvant therapy: a multireader study. Eur Radiol 2023;33(8):5761–5768.
13. Miranda J, Tan GXV, Fernandes MC, et al. Rectal MRI radiomics for predicting pathological complete response: Where we are. Clin Imaging 2022;82:141–149.
14. Di Re AM, Sun Y, Sundaresan P, et al. MRI radiomics in the prediction of therapeutic response to neoadjuvant therapy for locoregionally advanced rectal cancer: a systematic review. Expert Rev Anticancer Ther 2021;21(4):425–449.
15. Ke J, Jin C, Tang J, et al. A longitudinal MRI-based artificial intelligence system to predict pathological complete response after neoadjuvant therapy in rectal cancer: a multicenter validation study. Dis Colon Rectum 2023;66(12):e1195–e1206.
16. Jia LL, Zheng QY, Tian JH, et al. Artificial intelligence with magnetic resonance imaging for prediction of pathological complete response to neoadjuvant chemoradiotherapy in rectal cancer: A systematic review and meta-analysis. Front Oncol 2022;12:1026216.
17. Kim SH, Lee JM, Gupta SN, Han JK, Choi BI. Dynamic contrast-enhanced MRI to evaluate the therapeutic response to neoadjuvant chemoradiation therapy in locally advanced rectal cancer. J Magn Reson Imaging 2014;40(3):730–737.
18. Miranda J, Causa Andrieu P, Nincevic J, et al. Advances in MRI-based assessment of rectal cancer post-neoadjuvant therapy: a comprehensive review. J Clin Med 2023;13(1):172.
19. Brown G, Richards CJ, Newcombe RG, et al. Rectal carcinoma: thin-section MR imaging for staging in 28 patients. Radiology 1999;211(1):215–222.
20. Brown G, Radcliffe AG, Newcombe RG, Dallimore NS, Bourne MW, Williams GT. Preoperative assessment of prognostic factors in rectal cancer using high-resolution magnetic resonance imaging. Br J Surg 2003;90(3):355–364.
21. Kim TH, Firat C, Thompson HM, et al. Extramural venous invasion and tumor deposit at diffusion-weighted MRI in patients after neoadjuvant treatment for rectal cancer. Radiology 2023;308(2):e230079.
22. Yuval JB, Thompson HM, Firat C, et al. MRI at restaging after neoadjuvant therapy for rectal cancer overestimates circumferential resection margin proximity as determined by comparison with whole-mount pathology. Dis Colon Rectum 2022;65(4):489–496.
23. Zhang H, Zhang C, Zheng Z, et al. Chemical shift effect predicting lymph node status in rectal cancer using high-resolution MR imaging with node-for-node matched histopathological validation. Eur Radiol 2017;27(9):3845–3855.
24. Antunes J, Viswanath S, Brady JT, et al. Coregistration of preoperative MRI with ex vivo mesorectal pathology specimens to spatially map post-treatment

changes in rectal cancer onto in vivo imaging: preliminary findings. Acad Radiol 2018;25(7):833–841.
25. Pham TT, Stait-Gardner T, Lee CS, et al. Correlation of ultra-high field MRI with histopathology for evaluation of rectal cancer heterogeneity. Sci Rep 2019;9(1):9311.
26. Nougaret S, Reinhold C, Mikhael HW, Rouanet P, Bibeau F, Brown G. The use of MR imaging in treatment planning for patients with rectal carcinoma: have you checked the "DISTANCE"? Radiology 2013;268(2):330–344.
27. Beets-Tan RGH, Lambregts DMJ, Maas M, et al. Correction to: Magnetic resonance imaging for clinical management of rectal cancer: Updated recommendations from the 2016 European Society of Gastrointestinal and Abdominal Radiology (ESGAR) consensus meeting. Eur Radiol 2018;28(6):2711. [Published correction appears in Eur Radiol 2018;28(4):1465–1475.]
28. Fernandes MC, Gollub MJ, Brown G. The importance of MRI for rectal cancer evaluation. Surg Oncol 2022;43:101739.
29. Lambregts DMJ, Delli Pizzi A, Lahaye MJ, et al. A pattern-based approach combining tumor morphology on MRI with distinct signal patterns on diffusion-weighted imaging to assess response of rectal tumors after chemoradiotherapy. Dis Colon Rectum 2018;61(3):328–337.
30. Horvat N, El Homsi M, Miranda J, Mazaheri Y, Gollub MJ, Paroder V. Rectal MRI interpretation after neoadjuvant therapy. J Magn Reson Imaging 2023;57(2):353–369.
31. Ringel MJ, Heiselman JS, Richey WL, Meszoely IM, Jarnagin WR, Miga MI. Comparing regularized Kelvinlet functions and the finite element method for registration of medical images to sparse organ data. Med Image Anal 2024;96:103221.
32. Heiselman JS, Jarnagin WR, Miga MI. Intraoperative correction of liver deformation using sparse surface and vascular features via linearized iterative boundary reconstruction. IEEE Trans Med Imaging 2020;39(6):2223–2234.
33. Fitzpatrick JM, , Sonka M, eds. Handbook of Medical Imaging: vol 2, Medical image processing and analysis. Bellingham, Wash: SPIE, 2000.
34. Li L, Pahwa S, Penzias G, et al. Co-registration of ex vivo surgical histopathology and in vivo T2 weighted MRI of the prostate via multi-scale spectral embedding representation. Sci Rep 2017;7(1):8717.
35. Cimadamore A, Cheng L, Lopez-Beltran A, et al. Added clinical value of whole-mount histopathology of radical prostatectomy specimens: a collaborative review. Eur Urol Oncol 2021;4(4):558–569.
36. Sun C, Chatterjee A, Yousuf A, et al. Comparison of T2-weighted imaging, DWI, and dynamic contrast-enhanced MRI for calculation of prostate cancer index lesion volume: correlation with whole-mount pathology. AJR Am J Roentgenol 2019;212(2):351–356.
37. Trabulsi EJ, Calio BP, Kamel SI, et al. Prostate contrast enhanced transrectal ultrasound evaluation of the prostate with whole-mount prostatectomy correlation. Urology 2019;133:187–191.
38. Litjens GJ, Huisman HJ, Elliott RM, et al. Quantitative identification of magnetic resonance imaging features of prostate cancer response following laser ablation and radical prostatectomy. J Med Imaging (Bellingham) 2014;1(3):035001.
39. Rusu M, Rajiah P, Gilkeson R, et al. Co-registration of pre-operative CT with ex vivo surgically excised ground glass nodules to define spatial extent of invasive adenocarcinoma on in vivo imaging: a proof-of-concept study. Eur Radiol 2017;27(10):4209–4217.